Appl Magn Reson (2012) 43:237–250
DOI 10.1007/s00723-012-0364-3

Applied
Magnetic Resonance

Solvent-Free High-Field Dynamic Nuclear Polarization of Mesoporous Silica Functionalized with TEMPO

Aany Sofia Lilly Thankamony · Olivier Lafon · Xingyu Lu · Fabien Aussenac · Melanie Rosay · Julien Trébosc · Hervé Vezin · Jean-Paul Amoureux

Received: 7 March 2012 / Revised: 30 April 2012 / Published online: 4 June 2012

Abstract We report high-field magic-angle spinning dynamic nuclear polarization (MAS DNP) of mesoporous silica functionalized with nitroxide radicals. These results demonstrate that co-condensation can be employed to incorporate DNP polarizing agents into inorganic materials and that solvent-free DNP is feasible for porous materials. For the investigated material, the direct MAS DNP enhances the ^{29}Si nuclear magnetic resonance (NMR) spectra, whereas the indirect MAS DNP via protons is inapplicable owing to the inefficiency of $^{1}H \rightarrow {}^{29}Si$ cross polarization transfer. Furthermore, the ^{29}Si signals in direct experiments build up in a few seconds at 100 K. This fast polarization buildup improves the NMR sensitivity and will be useful for the investigation of direct DNP below 100 K.

A. S. Lilly Thankamony · O. Lafon (✉) · X. Lu · J. Trébosc · H. Vezin · J.-P. Amoureux
Univ. Lille Nord de France, 59000 Lille, France
e-mail: olivier.lafon@univ-lille1.fr

A. S. Lilly Thankamony · O. Lafon · X. Lu · J. Trébosc · J.-P. Amoureux
CNRS, UMR 8181, Unité de Catalyse et de Chimie du Solide, UCCS, Univ. Lille 1, Bât. C7, 59652 Villeneuve d'Ascq, France

F. Aussenac
Bruker BioSpin SA, 34, rue de l'Industrie, 67166 Wissembourg Cedex, France

M. Rosay
Bruker BioSpin Corporation, 15 Fortune Drive, Billerica, MA 01821, USA

H. Vezin
CNRS, UMR 8516, Laboratoire de Spectrochimie Infrarouge et Raman, LASIR, Univ. Lille 1, Bât. C4, 59652 Villeneuve d'Ascq, France

1 Introduction

Solid-state nuclear magnetic resonance (NMR) provides unique information on the atomic-scale structure and dynamics of heterogeneous, disordered or amorphous materials, such as heterogeneous catalysts [1], nuclear waste storage medium [2], battery related materials [3] and nanoobjects [4]. However, the intrinsic low sensitivity of NMR, resulting from the small nuclear magnetic moments, limits the observation of diluted species (interface sites, defects, reaction intermediates...) or of nuclei displaying low gyromagnetic ratio, low natural abundance and/or slow longitudinal nuclear relaxation. For instance, the observation of silicon sites can be limited by the low ^{29}Si natural abundance (4.7 %) and nuclear relaxation times (T_{1n}), which can reach several hours [5].

Dynamic nuclear polarization (DNP) is a promising method to enhance the NMR signal of materials by one or two orders of magnitude [6–19]. Since its invention, DNP has been applied to materials. DNP phenomenon at low static magnetic field, B^0, was initially reported in metals ($B^0 = 3$ mT) [6] and then semiconductors ($B^0 \approx 0.3$ T) [7]. For instance, low-field DNP has been applied for *n*-type silicon, amorphous silicon or hydrogenated amorphous silicon, using dangling bonds as endogenous polarizing agents [7, 9, 14]. The combination of DNP at $B^0 \approx 1.4$ T with magic-angle spinning (MAS) has allowed its application to carbonaceous materials, such as organic polymers, coals and diamonds [8, 10]. Furthermore, DNP-enhanced cross-polarization (CP) at $B^0 \approx 1.4$ T has been demonstrated in the 1990s for the selective observation of surfaces [11–13]. More recently, the development of stable high-frequency microwave (μw) source, gyrotrons [20], and the design of biradical polarizing agents [21] fostered the advent of DNP at high magnetic field with $B^0 \geq 5$ T. The improved resolution and the post-synthesis impregnation with nitroxide radical solution have permitted the extension of DNP to other material classes, including mesoporous silica [15–17], metal-oxide framework [18] and γ-alumina [19].

Dynamic nuclear polarization requires the presence of unpaired electrons in the sample. So far, high-field DNP studies of materials have mainly employed exogenous organic radicals, such as 4-amino-(2,2,6,6-tetramethylpiperidin-1-yloxyl) (4-amino-TEMPO) or 1-(TEMPO-4-oxy)-3-(TEMPO-4-amino)propan-2-ol (TOTAPOL), as a source of polarization. The radicals are introduced within the materials using post-synthesis impregnation with radical-containing solutions [15–17]. This protocol offers several advantages: (i) being a post-synthesis method, it does not alter the material preparation and can be planned for natural or already prepared samples; (ii) the protons of frozen solvents within the pores can be used for polarization distribution via ^{1}H–^{1}H spin diffusion; (iii) the presence of solvent may avoid the adsorption of the radicals onto the surface. Nevertheless, (i) it has only been demonstrated so far for materials displaying high specific surface area [15–19]; (ii) this protocol does not permit the accurate control of the position and the orientation of the paramagnetic agent with respect to the observed nuclei (only an average distance between the radical and the material surface can be inferred from the radical concentration [17]); (iii) the NMR signals of the solvents may overlap with those of the observed nuclei; (iv) the nature of the impregnation solvent affects

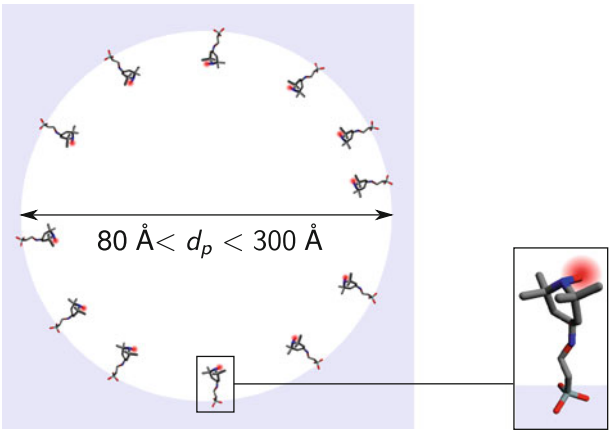

Fig. 1 Schematic structure of the material **1**

the DNP enhancements and, in practice, the sensitivity optimization still requires the test of different solvents [22].

Herein, we show how high-field DNP can be applied for paramagnetic materials containing endogenous radicals. We investigate an organic–inorganic hybrid material, which is mesoporous silica functionalized with TEMPO moieties, **1** (see Fig. 1) [23–25]. This hybrid material is a highly selective and effective oxidation heterogeneous catalyst for converting primary and secondary alcohol substrates into carbonyl derivatives and can be used for the production of pharmaceuticals, agrochemicals, flavors and fragrances [25–27]. These materials have also been used as polarizing agents for low-field DNP of flowing liquids using Overhauser effect [28, 29]. However, to the best of our knowledge, this type of material has never been studied by solid-state DNP/NMR. The TEMPO molecule is tethered to the silicon atoms during the material preparation by the sol–gel process. This co-condensation procedure can be advantageous, since: (i) it can be applied in principle to non-porous materials or microporous materials exhibiting pore aperture smaller than the smallest dimension of TEMPO and TOTAPOL (about 7 Å); (ii) it ensures a more homogeneous distribution of organic moieties within the inorganic material than post-synthesis incorporation [30]; (iii) the distance between the unpaired electrons and the silica surface cannot exceed 9 Å, the size of the organic moiety; (iv) this hybrid material allows solvent-free DNP to be tested since the xerogels are dried during the sample preparation [24]. This solvent-free DNP procedure demonstrated here for materials exhibits similarities with another solvent-free DNP protocol, which has been introduced recently for the DNP of polypeptides [31]. In this work, the molecular entities, unlabeled and labeled with nitroxide radicals, are co-condensed, whereas in reference [31], they were mixed by dissolution and solvent evaporation. In this article, the results of ^{1}H and ^{29}Si DNP experiments will be presented for **1** obtained using co-condensation. We will demonstrate that for this material, the cross-polarization (CP) transfer from ^{1}H to ^{29}Si nuclei is inefficient and hence the ^{29}Si nuclei cannot be polarized via ^{1}H (indirect DNP) [16]. Conversely,

we will show that the ^{29}Si NMR signal can be enhanced by direct polarization (DP) transfer from unpaired electrons (direct DNP) [17].

2 Materials and Methods

The material **1** was purchased from Sigma-Aldrich and was used without purification. It exhibits a high specific surface area of about 450 $m^2\ g^{-1}$ and broad pore size distribution with pore diameters ranging from 80 to 300 Å [24, 25].

X-band EPR experiments were performed using a Bruker BioSpin ELEXYS E580E spectrometer operating at 9.8 GHz. The spectra were recorded with 2 mW microwave power and 0.5 G of amplitude modulation. The spin concentration of the sample was determined by full spectral integration using 4-amino-TEMPO as a reference. The EPR spectra were recorded at room temperature and the sample of mesoporous silica functionalized with TEMPO was a powder.

All solid-state DNP MAS experiments were performed on a commercial Bruker BioSpin Avance III DNP spectrometer operating at a microwave frequency of 263 GHz, a static magnetic field, $B^0 = 9.393$ T and ^{1}H and ^{29}Si Larmor frequency of 399.87 and 79.44 MHz, respectively [32]. The wide-bore NMR magnet was equipped with a double resonance ^{1}H/X 3.2 mm low-temperature DNP MAS probe. The sample was placed in a 3.2-mm ZrO_2 rotor. Sample temperatures of 98 K were achieved and controlled under MAS condition using a Bruker BioSpin low-temperature MAS cooling system. The sample temperature corresponds to the calibrated temperature with microwave off. All the spectra were acquired at a MAS frequency, $\nu_r = 10$ kHz. During the DNP MAS experiment, a gyrotron generated continuous microwave irradiation, which was delivered to the sample by a corrugated waveguide. The microwave power at the position of the sample was approximately 6 W [32].

The ^{1}H and ^{29}Si NMR spectra enhanced by direct DNP were recorded using the pulse sequence described in ref. [17]. First, a presaturation suppresses the equilibrium Boltzmann polarization of the detected isotope. Then, the microwave irradiation during a time, $\tau_{\mu w}$, induces a transfer of longitudinal polarization between the unpaired electrons and the nuclei. The longitudinal polarization of ^{1}H or ^{29}Si nuclei is detected by tilting it into the *xy*-plane using radiofrequency pulses at the corresponding Larmor frequency. This pulse sequence relying on direct polarization (DP) is referred to as DP MAS in the following. The ^{1}H 90° pulse length was 2.5 µs in DP MAS ^{1}H experiment. All DP MAS ^{29}Si NMR spectra were recorded using a ^{29}Si 90° pulse length of 5 µs and background suppression to suppress the ^{29}Si signal of the probe [33]. The DP MAS ^{29}Si spectra of the investigated samples were unaffected by ^{1}H SPINAL-64 heteronuclear decoupling of 100 kHz amplitude [34]. Hence, no ^{1}H decoupling sequence was applied during DP MAS ^{29}Si experiments.

The indirect ^{29}Si DNP spectra were recorded using the usual ^{1}H → ^{29}Si CP MAS sequence but prior to the CP transfer, the longitudinal ^{1}H polarization was enhanced by microwave irradiation during a time, $\tau_{\mu w}$ [16]. The ^{1}H 90° pulse length was 2.5 µs. The CP transfer was performed using a contact time of 2 ms, a constant ^{29}Si rf nutation frequency of 50 kHz and a linear ramp of ^{1}H rf nutation frequency

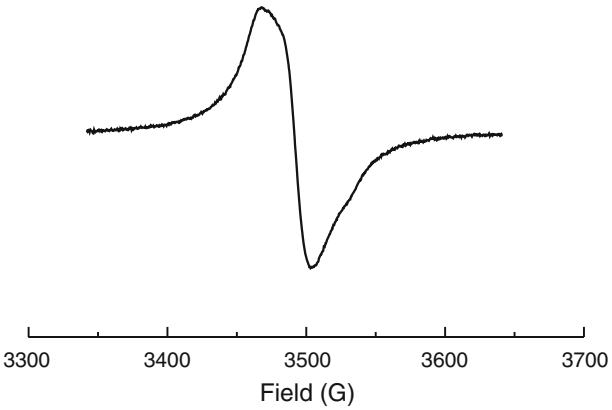

Fig. 2 X-band continuous wave EPR spectrum of the mesoporous silica functionalized with TEMPO

between 70 and 35 kHz. A SPINAL-64 decoupling with ^{1}H rf nutation frequency of 100 kHz was applied during the acquisition [34].

The ^{29}Si chemical shifts are referenced to tetramethylsilane using the shielded resonance (−9.8 ppm) in the ^{29}Si NMR spectrum of tetrakis(trimethylsilyl)silane as a secondary reference. For an isotope $X = {}^{1}\mathrm{H}$ or ^{29}Si, the DNP enhancement factors of the signal intensity and integral are defined as

$$\varepsilon_{\mathrm{DNP}}(X) = \frac{I(X)}{I_{\mathrm{off}}(X)} \quad \text{and} \quad \varepsilon^{A}_{\mathrm{DNP}}(X) = \frac{A(X)}{A_{\mathrm{off}}(X)}, \tag{1}$$

where the $I(X)$ and $I_{\mathrm{off}}(X)$ are the maximal intensities of X signal with and without microwave irradiation and the $A(X)$ and $A_{\mathrm{off}}(X)$ are the total integrals of X signal with and without microwave irradiation. For **1**, the intensities of ^{1}H and ^{29}Si signals peak at 0 and −66 ppm, respectively. The fit of NMR signals, as shown in Fig. 3d, was performed using Matlab software [35].

3 Results and Discussion

Figure 2 presents the EPR spectrum of the material **1** recorded at room temperature. The measured g factor is 2.0059, which is typical of nitroxide radical. The EPR spectrum of **1** displays a broad line exhibiting a shoulder at about 3,530 G. Therefore, it differs from the EPR signals of mononitroxide radicals in isotropic solution, which consist of a resolved triplet splitting produced by the isotropic hyperfine coupling with ^{14}N nucleus [21]. This difference indicates that the motions of the TEMPO moieties in material **1** are anisotropic. This is expected since the TEMPO moiety is anchored on the silica surface and its motions are limited by the covalent linkage. Furthermore, the EPR signal of **1** also differs from that of diluted mono- or bi-nitroxide radicals, which are immobilized in frozen glassy solutions or covalently linked to a peptide chain or to a silica surface [21, 23, 31, 36]. These diluted radicals show a resolved powder lineshape produced by the anisotropic

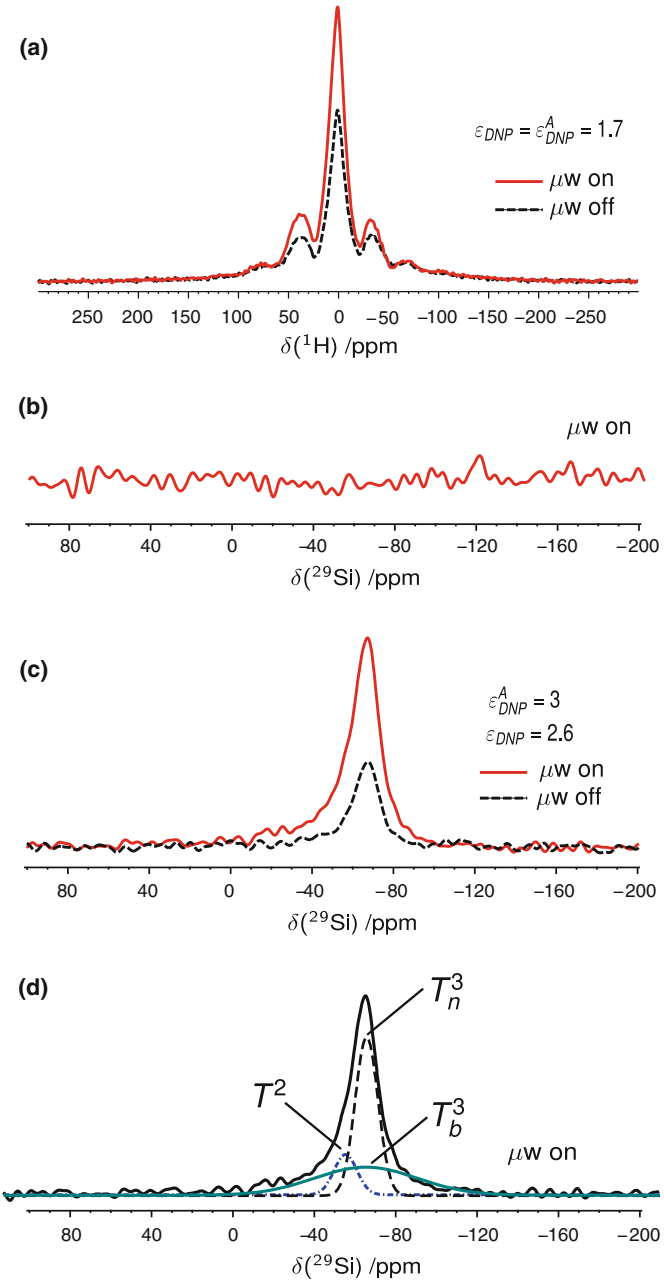

Fig. 3 Natural abundance ^{1}H and ^{29}Si NMR spectra of mesoporous silica functionalized with TEMPO. **a** DP MAS ^{1}H with (*top*) and without (*bottom*) microwave irradiation. The spectra were acquired with four scans and $\tau_{\mu w} = 5$ s. **b** CP MAS $^{1}H \rightarrow {}^{29}Si$ spectrum with microwave irradiation. The spectra were acquired with 64 scans and $\tau_{\mu w} = 10$ s. **c** DP MAS ^{29}Si NMR spectra with (*top*) and without (*bottom*) microwave irradiation. The spectra were acquired with 64 scans and $\tau_{\mu w} = 10$ s. **d** Deconvolution of the DP MAS ^{29}Si spectrum with microwave irradiation. The spectrum is identical to that displayed in **c**

hyperfine coupling with ^{14}N nucleus with a maximum A_{zz} component of about 65 G. For **1**, the powder lineshape is masked by the spectral broadening resulting from the extensive network of intermolecular dipolar couplings between the unpaired electrons. EPR measurements indicate that the TEMPO concentration of **1**, c_{m}, is about 70 mM. As the TEMPO moieties are grafted on the silica surface, it is also pertinent to estimate the TEMPO surface concentration in mol m^{-2} using

$$\Gamma = \frac{c_{\mathrm{m}}}{10^6 \rho a_s} \tag{2}$$

where c_m is expressed in mM, and $\rho = 0.4$ g cm^{-3} and $a_s = 456$ m^2 g^{-1} are the mass density and the specific surface area of **1**. Equation 2 yields $\Gamma = 380$ nmol m^{-2}. From Γ, the average distance R in Å between two TEMPO moieties can be estimated as

$$R = \left(\Gamma 10^{-20} \mathcal{N}_{\mathrm{A}}\right)^{-1/2} \tag{3}$$

assuming a 2-D square lattice for the positions of the TEMPO moieties. In Eq. 3, $\mathcal{N}_{\mathrm{A}}$ is the Avogadro number. The calculated R value is 19 Å for **1**.

The comparison of the EPR spectrum in Fig. 2 with those of diluted TEMPO moieties anchored on silica surface [23] indicates that the homogeneous spectral broadening arising from multiple dipolar couplings between electrons is comparable with the ^{29}Si Larmor frequency at 9.4 T (79.44 MHz). Therefore, the thermal mixing mechanism [8, 37, 38] can be involved in the DNP transfer for **1**, especially in the case of direct ^{29}Si DNP.

Figure 3a shows the one-dimensional (1D) ^{1}H NMR spectrum of **1** with and without microwave irradiation. For both spectra, the maximum intensity is observed at $\delta \approx 0$ ppm, which is typical of ^{1}H in alkyl groups linked to silicon atoms. As the material **1** is obtained by co-condensation of 4-oxo-TEMPO, aminopropyltrimethoxysilane and methyltrimethoxysilane [23–25], the silica surface is functionalized with methyl and (4-TEMPO)aminopropyl groups, as shown in Fig. 1. The silica surface must also contain silanol protons (Si-OH), but their ^{1}H signals between 1 and 8 ppm (2 ppm for non-hydrogen-bonded silanol) [39] is not resolved from that of alkyl protons.

The second moment, $M_2(\nu_r)$, of ^{1}H signal at MAS frequency of 10 kHz was calculated as [40, 41]

$$M_2(\nu_r) = \frac{1}{A}\int_{\nu_i}^{\nu_s} (\nu - \nu_0)^2 I(\nu) \mathrm{d}\nu \tag{4}$$

where the ν_i and ν_s frequencies are the lower and upper bounds of the frequency interval in which the ^{1}H signal intensity exceeds the noise, A the integral of ^{1}H signal between ν_i and ν_s frequencies, ν is the frequency, ν_0 is the frequency of the maximum in intensity, and $I(\nu)$ the ^{1}H signal intensity at the frequency ν. For **1**, the $M_2(\nu_r)$ value is about 300 kHz^2 and the square root of the $M_2(\nu_r)$, which is proportional to full width at half maximum for a Gaussian lineshape, is twofold lower in absolute value for **1** than those measured for 10 %-protonated frozen

solvents contained within the pores of mesoporous silica. This observation is consistent with an averaging of the ^{1}H–^{1}H dipolar couplings in **1** by the threefold hopping of the methyl groups [42], the librational motion of the O–H groups about the Si–O axes [43] and the conformational changes of (4-TEMPO)aminopropyl chains [44–46]. When the pores of mesoporous silica do not contain solvents, the rate of these motions at about 100 K is faster than 1 MHz, i.e., their correlation time is below 1 μs [43–46]. As most protons experience fast librational motions and the grafted TEMPO moieties are mobile in the silica pores, the electron–proton interactions are time dependent. Nevertheless, at $B^0 = 9.393$ T and 100 K, polarization of protons via Overhauser effect [47] is unlikely since the spectral density of molecular motions in dielectric solids is very low at about 263 GHz, the electron Larmor frequency [48].

As the full width at half maximum is proportional to the square root of the $M_2(\nu_r)$ [40, 49] and the full width at half maximum of the ^{1}H signal is inversely proportional to ν_r [49, 50], the second moment under static conditions, $M_2(0)$, can be calculated as

$$M_2(0) = \frac{\nu_r}{K}[M_2(\nu_r)]^{1/2} \tag{5}$$

where the dimensionless K constant lies in the range [0.04, 0.1] [50]. The average dipolar coupling constant between protons, $\overline{b}_{\mathrm{HH}}/(2\pi)$, can be deduced from the square root of the $M_2(0)$ [51]

$$\frac{\overline{b}_{\mathrm{HH}}}{2\pi} = -\frac{2}{3}\left[\frac{M_2(0)}{\chi}\right]^{1/2} \tag{6}$$

where χ is a structural factor, which depends on the proton distribution in the sample. Here, given that (i) the protons are located on the pore surfaces, (ii) the pore average radius is much larger than the average ^{1}H–^{1}H distance between nearest neighbors, we can assume a 2-D square lattice of protons and hence $\chi = 4.77$ [51]. For the investigated systems, the electron longitudinal relaxation times, T_{1e}, are shorter than the ^{1}H transverse longitudinal relaxation times ($T_{1e} < T_{2n}(^{1}\mathrm{H})$), and the radius of the spin diffusion barrier, r_{d}, can be calculated as [52]

$$r_{\mathrm{d}} \approx \left[2S\frac{\gamma_e}{\gamma(^{1}\mathrm{H})}B_S\left(\frac{S\hbar\gamma_e B^0}{k_{\mathrm{B}}T}\right)\right]^{\alpha}\left|\frac{\mu_0}{4\pi}\frac{\gamma^2(^{1}\mathrm{H})\hbar}{\overline{b}_{\mathrm{HH}}}\right|^{1/3} \tag{7}$$

where $S = 1/2$ is the effective spin quantum number for the unpaired electron of TEMPO monoradical, γ_e and $\gamma(^{1}\mathrm{H})$ are the gyromagnetic ratios of electron and ^{1}H nucleus, B_S the Brillouin function with parameter S, $\hbar$ is the reduced Planck constant, k_{B} the Boltzmann constant, $T = 98$ K the sample temperature and $\alpha = 1/4$ using Khutsishvili's definition of the diffusion barrier [17, 52]. According to Eq. 7, the r_{d} value lies in the range [4.6, 5.4 Å], which is consistent with diffusion barrier radii reported in the literature [53]. Furthermore, the r_{d} radius is shorter than R and as the protons are located on the silica surface, the fraction, f_{d}, of protons enclosed within the diffusion barrier is given by

$$f_d = \frac{\pi r_d^2}{R^2}. \quad (8)$$

The calculated f_d value lies between 18 and 25 %, indicating that a significant fraction of protons is not involved in the polarization transfer via ^{1}H–^{1}H spin diffusion in the direct ^{1}H DNP.

Figure 3a shows limited DNP enhancement of ^{1}H signal intensity ($\varepsilon_{DNP}(^1H) = 1.7$). This limited enhancement mainly stems from: (i) the lower efficiency of monoradicals at high field for ^{1}H signal enhancement compared to that of biradicals [21, 54–56]; (ii) the weak ^{1}H–^{1}H dipolar couplings in **1**, which result in slow proton spin diffusion and hinder the distribution of ^{1}H polarization within the sample [57, 58]; (iii) the short electron and proton relaxation times in **1** owing to the high molecular mobility, the presence of paramagnetic molecular oxygen and the high concentration of unpaired electrons [21, 59, 60]. Short electron longitudinal relaxation times (T_{1e}) reduce the saturation of EPR transition, whereas short nuclear longitudinal relaxation times (T_{1n}) limit the time to "pump" the nuclear polarization. The ^{1}H lineshape is unaffected by the DNP transfer and the enhancement of signal integral is equal to that of signal intensity ($\varepsilon_{DNP}(^1H) = \varepsilon^A_{DNP}(^1H)$). This result is consistent with the homogeneous broadening of the ^{1}H signal [61].

Figure 3b shows the 1D CP MAS ^{1}H → ^{29}Si spectrum of **1** with microwave irradiation. No ^{29}Si signal is visible after 64 scans. This observation indicates that the ^{1}H → ^{29}Si CP transfer is inefficient for **1**. This inefficiency does not stem from an interference between the conformational dynamics and the ^{1}H heteronuclear decoupling [42, 62, 63], since the ^{29}Si signal intensity in DP MAS experiment was not affected on applying a ^{1}H heteronuclear decoupling of 100 kHz amplitude. This result is consistent with conformational dynamics in **1** faster than 1 MHz at about 100 K, in the absence of solvent molecules in the silica pores [44–46]. The inefficiency of ^{1}H → ^{29}Si CP transfer mainly results from (i) the short nuclear longitudinal relaxation times in the rotating frame, $T_{1\rho}$, owing to the high concentration of TEMPO moieties [64] and (ii) the weak ^{1}H–^{29}Si dipolar couplings, which are partly averaged out by the conformational dynamics.

Conversely, as shown in Fig. 3c, the ^{29}Si direct experiments allow the detection of a ^{29}Si signal in a few minutes with and without microwave irradiation. The high sensitivity of these experiments stems from the fast polarization buildup. The fast signal buildup in direct DNP is discussed below (see Fig. 4). In the absence of microwave irradiation, the longitudinal ^{29}Si magnetization of **1** builds up in a few seconds, whereas in mesoporous silica containing frozen solvents and nitroxide radicals, the longitudinal ^{29}Si relaxation requires thousands of seconds. The faster relaxation for **1** results from (i) the shorter average distance between unpaired electrons and ^{29}Si nuclei, which is constrained by the covalent linkage [65–67] and (ii) the higher mobility at the atomic scale in the absence of frozen solvents in the pores. Furthermore, direct ^{29}Si DNP yields DNP enhancements, $\varepsilon_{DNP}(^{29}Si) = 2.6$ and $\varepsilon^A_{DNP}(^{29}Si) = 3$, which are more than 50 % higher than those measured for direct ^{1}H DNP. The higher signal enhancements in direct ^{29}Si DNP compared to direct ^{1}H DNP are consistent with the theoretical maximal enhancements [17, 68, 69], which are given by the ratios $\gamma_e/\gamma(^{29}Si) \approx 3311$ for ^{29}Si and $\gamma_e/\gamma(^1H) \approx 658$ for

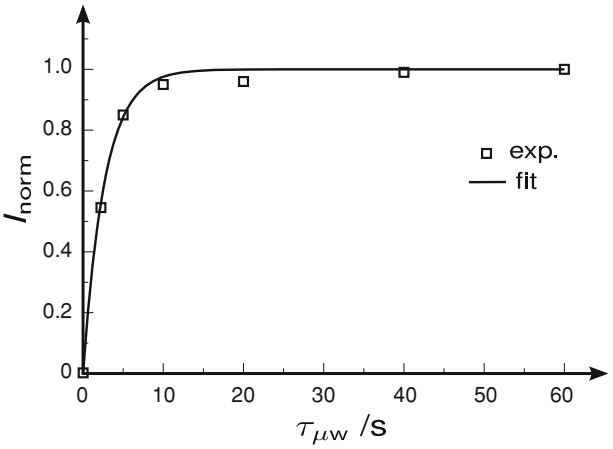

Fig. 4 Buildup curve of DP ^{29}Si signal intensity with microwave irradiation as function of $\tau_{\mu w}$ delay. The signal intensities, $I(\tau_{\mu w})$, are normalized with respect to the signal intensities at $\tau_{\mu w} = 60$ s: $I_{norm} = I(\tau_{\mu w})/I(60)$. The experimental points and the fit according to Eq. 9 are displayed as *square symbols* and *continuous line*, respectively.

^{1}H, where $\gamma(^{29}\mathrm{Si})$ is the gyromagnetic ratio of the ^{29}Si nucleus. Nevertheless, the direct ^{29}Si DNP enhancement is lower for **1** than those measured for mesoporous silica containing frozen solutions of nitroxide radicals within its pores [17]. For instance, $|\varepsilon_{DNP}|$ values of 11 and 30 were measured for mesoporous silica containing 30 mM of 4-amino-TEMPO and 15 mM of TOTAPOL in [$^2H_6$]-DMSO/^2H_2O/H_2O frozen matrix [17]. The lower $\varepsilon_{DNP}(^{29}\mathrm{Si})$ values for **1** stem from different factors. First, the polarization transfer in **1** relies mainly on mono-radical TEMPO, whereas the biradicals, such as TOTAPOL, are usually more efficient at high field [21, 54–56]. Second, in this work, DNP experiments were performed at a B^0 value, which is optimal for direct ^{1}H DNP employing nitroxide radicals but not optimal for the direct polarization of isotopes with low gyromagnetic ratios [17, 68, 69]. Third, as explained above for ^{1}H DNP, the electron and nuclear relaxations must be faster in **1** than in mesoporous silica impregnated with frozen solutions. However, the faster nuclear relaxation also leads to faster polarization buildup, which is a significant advantage in terms of sensitivity, as shown below.

The difference between $\varepsilon_{DNP}(^{29}\mathrm{Si})$ and $\varepsilon^A_{DNP}(^{29}\mathrm{Si})$ arises from the broader foot of the DP ^{29}Si signal with microwave irradiation compared to that without microwave irradiation. This broad ^{29}Si signal corresponds to silicon-29 nuclei experiencing large hyperfine interaction and which are located in the vicinity of the unpaired electrons. Therefore, in direct ^{29}Si DNP, the polarization of the silicon-29 nuclei close to the TEMPO moiety is higher than that of remote ^{29}Si nuclei. Similar observations have been reported for ^{13}C direct DNP at low magnetic field [8].

The DP ^{29}Si signal displays a maximum at −66 ppm, the chemical shift of $R\mathrm{Si(OSi)_3}$ sites (T^3) with $R = CH_3$ or (4-TEMPO)aminopropyl groups [70, 71]. No ^{29}Si signal is observed in the chemical shift range, −110 to −90 ppm, corresponding to $(\mathrm{SiO})_n\mathrm{Si(OH)}_{4-n}$ (Q^n) sites. This observation proves that all Si

atoms are covalently linked to a carbon atom in **1**, which is consistent with the preparation of **1** from aminopropyltrimethoxysilane and methyltrimethoxysilane precursors. Furthermore, the ^{29}Si signal is asymmetrical and cannot be fitted by a single Gaussian lineshape. In a phenomenological approach, the DP ^{29}Si signal with microwave irradiation has been fitted as the sum of three Gaussian lineshapes: T_n^3, T_b^3 and T^2 (see Fig. 3d). Similar deconvolution has been used to fit the DP ^{29}Si signal without microwave irradiation (not shown). The T^2 contribution corresponds to the RSi(OSi)$_2$OH sites with $R = CH_3$ or (4-TEMPO)aminopropyl groups. In the fit, the average chemical shift of T^2 sites was fixed to −57 ppm [70, 71]. The introduction of T_n^3 contribution was necessary to obtain a reasonable fit of the signal foot. The T_b^3 contribution corresponds to the signal of T^3 sites close to a TEMPO moiety, whereas the T_n^3 contribution subsumes the signals of other T^3 sites. The boundary between T_n^3 and T_b^3 sites is not well defined, since there are several sources of line broadening, including the bulk magnetic susceptibility effect, which is difficult to estimate [72]. Furthermore, to better constrain the fit, identical full widths at half maximum have been used for T^2 and T_n^3 sites. The integral of T_n^3 contribution is about fivefold larger than that of T^2 contribution with or without microwave irradiation. Conversely, the relative area of T_b^3 contribution increases from 30 % without microwave irradiation to 40 % with microwave irradiation. This observation confirms the higher polarization of T_b^3 sites close to unpaired electrons in direct ^{29}Si DNP.

Figure 4 shows that the DNP-enhanced DP ^{29}Si signal intensity builds up in less than 10 s. We propose to model the buildup of ^{29}Si signals in direct DNP experiments as a stretched exponential function

$$I_{\text{norm}} = I_{\text{norm}}^{\infty}\left\{1 - \exp\left[-\left(\frac{\tau_{\mu w}}{\tau_{\text{DNP}}}\right)^{1/2}\right]\right\} \tag{9}$$

where $\tau_{\text{DNP}} = 1.3$ s is the DNP buildup time constant and I_{norm}^{∞} is the asymptotic normalized intensity for $\tau_{\mu w} \gg \tau_{\text{DNP}}$. This model is proposed since the direct ^{29}Si DNP does not involve ^{29}Si–^{29}Si spin diffusion and the polarization is transferred directly via electron-^{29}Si hyperfine interactions. The same interactions govern the nuclear relaxation via paramagnetic centers in the absence of nuclear spin diffusion and for randomly distributed impurities in a 3-D space, this relaxation mechanism results in a buildup of nuclear polarization, which follows an exponential function of $\sqrt{t}$ [73, 74]. Therefore, it is reasonable to postulate analogous buildup in direct ^{29}Si DNP. Compared to a biexponential model employed in ref. [17], the stretched exponential model has the advantage of assuming a continuous increase of the buildup time with increasing distances to the paramagnetic centers.

The value of $\tau_{\text{DNP}} = 1.3$ s for **1** is much shorter than the buildup times reported for direct ^{29}Si DNP on mesoporous silica containing nitroxide radicals in frozen solution (about 4,000 s) [17]. This difference in τ_{DNP} values represents a sensitivity gain by a factor $(4{,}000/1.3)^{1/2} \approx 55$, which counterbalances the lower DNP enhancements for solvent-free DNP; and the global DNP enhancement [31] could be larger for **1** than for mesoporous silica containing frozen solvent.

4 Conclusion

We demonstrated that co-condensation is supplementary to post-synthesis impregnation for the incorporation of DNP polarizing agents into inorganic materials. Using this protocol, the ^{29}Si NMR signals of functionalized mesoporous silica was enhanced by high-field direct ^{29}Si DNP. We also proved the feasibility of solvent-free DNP for porous materials. The functionalization of materials with nitroxide radicals allows the removal of solvent molecules from the pores. Even if the reported DNP enhancements are limited, the polarization buildups with and without microwave irradiation are fast, which is a significant advantage in terms of sensitivity. This fast buildup is promising for DNP experiments below 100 K, since the T_{1n} times are usually long at low temperatures [75, 76]. The direct DNP is shown to be an alternative to indirect DNP, when the CP transfer is inefficient. Therefore, the direct DNP will be useful for systems featuring high atomic mobility or high concentration in unpaired electrons. The DNP enhancement for direct ^{29}Si can be improved by (i) grafting TOTAPOL derivatives, instead of TEMPO moieties, in order to benefit from the efficient cross-effect mechanism; (ii) the optimization of B^0 field and radical concentration; (iii) the use of sapphire rotor instead of ZrO_2 rotors since the sapphire is nearly transparent to the 263 GHz of microwave irradiation [32]. It would be also worth studying the influence of the nitroxide position and dynamics by varying the length and the flexibility of the linkage between the nitroxide radical and the silica surface. The impregnation of **1** with organic solvents will permit to distinguish the effects of frozen solvent presence within the pores and radical grafting on the enhancement in direct and indirect DNP experiments. The further studies proposed above are currently in progress.

Acknowledgments The authors are grateful for funding provided by Region Nord/Pas de Calais, Europe (FEDER), CNRS, French Minister of Science, FR-3050, USTL, ENSCL, Bruker BIOSPIN, and Contract No. ANR-2010-JCJC-0811-01.

References

1. K. Na, C. Jo, J. Kim, K. Cho, J. Jung, Y. Seo, R.J. Messinger, B.F. Chmelka, R. Ryoo, Science **333**, 328 (2011)
2. I. Farnan, H. Cho, W.J. Weber, Nature **445**, 190 (2007)
3. B. Key, R. Bhattacharyya, M. Morcrette, V. Seznéc, J.M. Tarascon, C.P. Grey, J. Am. Chem. Soc. **131**, 9239 (2009)
4. S. Cadars, B.J. Smith, J.D. Epping, S. Acharya, N. Belman, Y. Golan, B.F. Chmelka, Phys. Rev. Lett. **103**, 136802 (2009)
5. J.S. Hartman, A. Narayanan, Y. Wang, J. Am. Chem. Soc. **116**, 4019 (1994)
6. T.R. Carver, C.P. Slichter, Phys. Rev. **92**, 212 (1953)
7. A. Abragam, J. Combrisson, I. Solomon, C. R. Acad. Sci. **246**, 1035 (1958)
8. R. Wind, M. Duijvestijn, C. van der Lugt, A. Manenschijn, J. Vriend, Prog. Nucl. Magn. Reson. Spectrosc. **17**, 33 (1985)
9. H. Lock, R. Wind, G. Maciel, N. Zumbulyadis, Solid State Commun. **64**, 41 (1987)
10. M. Afeworki, J. Schaefer, Macromolecules **25**, 4097 (1992)
11. H. Lock, G.E. Maciel, C.E. Johnson, J. Mater. Res. **7**, 2791 (1992)
12. H. Lock, R.A. Wind, G.E. Maciel, C.E. Johnson, J. Chem. Phys. **99**, 3363 (1993)

13. R.A. Wind, in Encyclopedia of Magnetic Resonance, ed. by R.K. Harris, R.E. Wasylishen (Wiley, Ltd, Chichester, published online 15th March 2007). doi:10.1002/9780470034590.emrstm0140
14. A.E. Dementyev, D.G. Cory, C. Ramanathan, Phys. Rev. Lett. **100**, 127601 (2008)
15. A. Lesage, M. Lelli, D. Gajan, M.A. Caporini, V. Vitzthum, P. Miéville, J. Alauzun, A. Roussey, C. Thieuleux, A. Mehdi, G. Bodenhausen, C. Copéret, L. Emsley, J. Am. Chem. Soc. **132**, 15459 (2010)
16. M. Lelli, D. Gajan, A. Lesage, M.A. Caporini, V. Vitzthum, P. Miéville, F. Héroguel, F. Rascón, A. Roussey, C. Thieuleux, M. Boualleg, L. Veyre, G. Bodenhausen, C. Copéret, L. Emsley, J. Am. Chem. Soc. **133**, 2104 (2011)
17. O. Lafon, M. Rosay, F. Aussenac, X. Lu, J. Trébosc, O. Cristini, C. Kinowski, N. Touati, H. Vezin, J.P. Amoureux, Angew. Chem. Int. Ed **50**, 8367 (2011)
18. A.J. Rossini, A. Zagdoun, M. Lelli, J. Canivet, S. Aguado, O. Ouari, P. Tordo, M. Rosay, W.E. Maas, C. Copéret, D. Farrusseng, L. Emsley, A. Lesage, Angew. Chem. Int. Ed **51**, 123 (2012)
19. V. Vitzthum, P. Mieville, D. Carnevale, M.A. Caporini, D. Gajan, C. Copéret, M. Lelli, A. Zagdoun, A.J. Rossini, A. Lesage, L. Emsley, G. Bodenhausen, Chem. Commun. **48**, (2012)
20. L.R. Becerra, G.J. Gerfen, R.J. Temkin, D.J. Singel, R.G. Griffin, Phys. Rev. Lett. **71**, 3561 (1993)
21. C. Song, K.N. Hu, C.G. Joo, T.M. Swager, R.G. Griffin, J. Am. Chem. Soc. **128**, 11385 (2006)
22. A. Zagdoun, A.J. Rossini, D. Gajan, A. Bourdolle, O. Ouari, M. Rosay, W.E. Maas, P. Tordo, M. Lelli, L. Emsley, A. Lesage, C. Coperet, Chem. Commun. **48**, 654 (2012)
23. R. Ciriminna, J. Blum, D. Avnir, M. Pagliaro, Chem. Commun. pp. 1441–1442 (2000)
24. R. Ciriminna, C. Bolm, T. Fey, M. Pagliaro, Adv. Synth. Catal. **344**, 159 (2002)
25. A. Michaud, G. Gingras, M. Morin, F. Béland, R. Ciriminna, D. Avnir, M. Pagliaro, Org. Process Res. Dev. **11**, 766 (2007)
26. R. Ciriminna, M. Pagliaro, Org. Process Res. Dev. **14**, 245 (2009)
27. L. Tebben, A. Studer, Angew. Chem. Int. Ed **50**, 5034 (2011)
28. H. Dorn, T. Glass, R. Gitti, K. Tsai, Appl. Magn. Reson. **2**, 9 (1991)
29. E.R. McCarney, S. Han, J. Magn. Reson. **190**, 307 (2008)
30. M.H. Lim, A. Stein, Chem. Mater. **11**, 3285 (1999)
31. V. Vitzthum, F. Borcard, S. Jannin, M. Morin, P. Miéville, M.A. Caporini, A. Sienkiewicz, S. Gerber-Lemaire, G. Bodenhausen, ChemPhysChem **12**, 2929 (2011)
32. M. Rosay, L. Tometich, S. Pawsey, R. Bader, R. Schauwecker, M. Blank, P.M. Borchard, S.R. Cauffman, K.L. Felch, R.T. Weber, R.J. Temkin, R.G. Griffin, W.E. Maas, Phys. Chem. Chem. Phys. **12**, 5850 (2010)
33. D.G. Cory, W.M. Ritchey, J. Magn. Reson. **80**, 128 (1988)
34. B.M. Fung, A.K. Khitrin, K. Ermolaev, J. Magn. Reson. **142**, 97 (2000)
35. Mathworks Inc. http://www.mathworks.com
36. D. Baute, V. Frydman, H. Zimmermann, S. Kababya, D. Goldfarb, J. Phys. Chem. B **109**, 7807 (2005)
37. V.A. Atsarkin, Sov. Phys. Solid State **21**, 725 (1978)
38. C.T. Farrar, D.A. Hall, G.J. Gerfen, S.J. Inati, R.G. Griffin, J. Chem. Phys. **114**, 4922 (2001)
39. C.E. Bronnimann, R.C. Zeigler, G.E. Maciel, J. Am. Chem. Soc. **110**, 2023 (1988)
40. A. Abragam, The Principles of Nuclear Magnetism (Oxford University Press, Oxford, 1961)
41. D. Hirsemann, T.K.J. Koster, J. Wack, L. van Wullen, J. Breu, J. Senker, Chem. Mater. **23**, 3152 (2011)
42. V.S. Bajaj, P.C. van der Wel, R.G. Griffin, J. Am. Chem. Soc. **131**, 118 (2008)
43. T. Kobayashi, J.A. DiVerdi, G.E. Maciel, J. Phys. Chem. C **112**, 4315 (2008)
44. E.C. Kelusky, C.A. Fyfe, J. Am. Chem. Soc. **108**, 1746 (1986)
45. R.C. Zeigler, G.E. Maciel, J. Am. Chem. Soc. **113**, 6349 (1991)
46. R.C. Zeigler, G.E. Maciel, J. Phys. Chem. **95**, 7345 (1991)
47. A.W. Overhauser, Phys. Rev. **92**, 411 (1953)
48. C. Griesinger, M. Bennati, H. Vieth, C. Luchinat, G. Parigi, P. Hfer, F. Engelke, S. Glaser, V. Denysenkov, T. Prisner, Prog. Nucl. Magn. Reson. Spectrosc. (2012, in press)
49. E. Brunner, D. Freude, B. Gerstein, H. Pfeifer, J. Magn. Reson. **90**, 90 (1990)
50. V.E. Zorin, S.P. Brown, P. Hodgkinson, J. Chem. Phys. **125**, 144508 (2006)
51. D.H. Levy, K.K. Gleason, J. Phys. Chem. **96**, 8125 (1992)
52. G.R. Khutsishvili, Phys. Usp. **11**, 802 (1969)
53. C. Ramanathan, Appl. Magn. Reson. **34**, 409 (2008)
54. C.F. Hwang, D.A. Hill, Phys. Rev. Lett. **19**, 1011 (1997)

55. K.N. Hu, C. Song, H.H. Yu, T.M. Swager, R.G. Griffin, J. Chem. Phys. **128**, 052302 (2008)
56. K.N. Hu, G.T. Debelouchina, A.A. Smith, R.G. Griffin, J. Chem. Phys. **134**, 125105 (2011)
57. M. Rosay, A.C. Zeri, N.S. Astrof, S.J. Opella, J. Herzfeld, R.G. Griffin, J. Am. Chem. Soc. **123**, 1010 (2001)
58. P.C.A. van der Wel, K.N. Hu, J. Lewandowski, R.G. Griffin, J. Am. Chem. Soc. **128**, 10840 (2006)
59. K.N. Hu, Solid State Nucl. Magn. Reson. **40**, 31 (2011)
60. A. Zagdoun, G. Casano, O. Ouari, G. Lapadula, A.J. Rossini, M. Lelli, M. Baffert, D. Gajan, L. Veyre, W.E. Maas, M. Rosay, R.T. Weber, C. Thieuleux, C. Copéret, A. Lesage, P. Tordo, L. Emsley, J. Am. Chem. Soc. **134**, 2284 (2011)
61. M.M. Maricq, J.S. Waugh, J. Chem. Phys. **70**, 3300 (1979)
62. W.P. Rothwell, J.S. Waugh, J. Chem. Phys. **74**, 2721 (1981)
63. A.H. Linden, S. Lange, W.T. Franks, Ü. Akbey, E. Specker, van B.J. Rossum, H. Oschkinat, J. Am. Chem. Soc. **133**, 19266 (2011)
64. S. Lange, A.H. Linden, Akbey, W. Trent Franks, N.M. Loening, B.J.v. Rossum, H. Oschkinat, J. Magn. Reson. **216**, 209 (2012)
65. N.P. Wickramasinghe, M. Kotecha, A. Samoson, J. Past, Y. Ishii, J. Magn. Reson. **184**, 350 (2007)
66. N.P. Wickramasinghe, S. Parthasarathy, C.R. Jones, C. Bhardwaj, F. Long, M. Kotecha, S. Mehboob, L.W.M. Fung, J. Past, A. Samoson, Y. Ishii, Nat. Meth. **6**, 215 (2009)
67. P.S. Nadaud, J.J. Helmus, I. Sengupta, C.P. Jaroniec, J. Am. Chem. Soc. **132**, 9561 (2010)
68. T. Maly, L.B. Andreas, A.A. Smith, R.G. Griffin, Phys. Chem. Chem. Phys. **12**, 5872 (2010)
69. T. Maly, A.F. Miller, R.G. Griffin, ChemPhysChem **11**, 999 (2010)
70. C.A. Fyfe, Y. Zhang, P. Aroca, J. Am. Chem. Soc. **114**, 3252 (1992)
71. B. Dietrich, K. Holtin, M. Bayer, V. Friebolin, M. Kühnle, K. Albert, Anal. Bioanal. Chem. **391**, 2627 (2008)
72. G. Kervern, G. Pintacuda, Y. Zhang, E. Oldfield, C. Roukoss, E. Kuntz, E. Herdtweck, J.M. Basset, S. Cadars, A. Lesage, C. Copéret, L. Emsley, J. Am. Chem. Soc. **128**, 13545 (2006)
73. D. Tse, S.R. Hartmann, Phys. Rev. Lett. **21**, 511 (1968)
74. D. Tse, I.J. Lowe, Phys. Rev. **166**, 292 (1968)
75. K.R. Thurber, W.M. Yau, R. Tycko, J. Magn. Reson. **204**, 303 (2010)
76. Y. Matsuki, K. Ueda, T. Idehara, R. Ikeda, K. Kosuga, S. Nakamura, M. Toda, T. Anai, T. Fujiwara, in Third International DNP Symposium on dynamic nuclear polarization (Lausanne, 2011)